3D MULTIPLE CRACK SYSTEM: EXTRACTION AND ANALYSIS USING MOTION-BASED IMAGE PROCESSING TECHNIQUE

T. Zhang [1], E. Nagy [2] (Member, ASCE), E. Landis [3] (Member, ASCE), and G. Nagy [4]

ABSTRACT

We present a motion-based method to extract the multiple 3D crack surfaces from a sequence of 3D X-ray microtomographic mortar images. We verify the correctness and accuracy of results by ground truth obtained with simulated cracks in real specimens. We provide several three-dimensional measures of crack surface, including the number of cracks, surface area, volume, tortuosity, and permeability.

Keywords: X-ray microtomography, image processing, concrete fracture.

INTRODUCTION

We examine the crack surfaces of concrete fracture by image processing. Although it is known that microstructural processes ultimately govern the fracture behavior of concrete, they have been ignored because "understanding of this problem is particularly weak" (Bažant 1995). Most previous research was conducted in 2D by analyzing the jagged contours of cracks. The results indicate that two-dimensional models are not effective in investigating concrete, which exhibits complex 3D fracture surfaces.

X-ray microtomography produces a three-dimensional representation of the internal structures of a concrete specimen at an unprecedented resolution (Landis et al. 1999). By applying increasing compressive loads to a specimen, this technique generates multiple volumetric images that capture the fracture evolution. We acquire, from these images, the crack surfaces and provide some 3D measurements for characterizing the fracture process.

In the following, we first explain this method. We evaluate the method and describe the types of measurements. We then present the results on two sequences of concrete images at the 6-μm resolution. We conclude our paper by summarizing our findings.

MOTION-BASED METHOD TO RECOVER CRACK SURFACES

This method recovers the crack surfaces in three steps. (a) *Preprocessing* locates the concrete region of interest. (b) *Motion estimation* obtains a 3D displacement vector field between pairs of images. (c) *Motion segmentation* recovers the multiple fractured segments by grouping the displacement vectors. For efficiency, the last two steps are iterated in a multi-resolution

[1]Rensselaer Polytechnic Institute, Troy, NY 12180, USA, email: zhant@rpi.edu

[2]University of Maine, Orono, Maine 04469, USA, email: edwin.nagy@maine.edu

[3]University of Maine, Orono, Maine 04469, USA, email: landis@maine.edu

[4]Rensselaer Polytechnic Institute, Troy, NY 12180, USA, email: nagy@ecse.rpi.edu

scheme that takes advantage of results at a lower resolution to process the data at the next higher resolution. A long image sequence is processed using an incremental scheme. Finally the triangulated surface meshes of cracks are generated by finding the boundaries between neighboring fragments. A diagram of the method is in Figure 1. Each step is briefly discussed next, with additional details in (Zhang 2004).
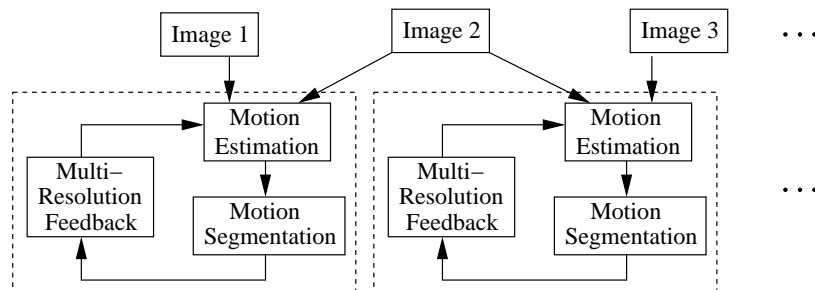
FIG. 1.   The diagram of identifying crack surfaces from a sequence of images.

Preprocessing: The original images of concrete have different sizes, and exhibit large areas of dark background without concrete. We first crop each image to a uniform size, large enough to cover the whole concrete region, by resampling around its centroid. A 'shrink-wrapping' procedure, implemented using a fast-marching level-set method (Malladi et al. 1995), is applied to obtain the concrete region of interest.

Motion Estimation: Block-matching (Konrad 2000) is used to estimate a 3D displacement vector field between two images. In addition to adapting the Sequential Similarity Detection Algorithm (SSDA) (Barnea and Silverman 1972) to 3D, we speed it up by restricting the number of voxels in the search window and the size of the search space.

Motion Segmentation: The neighboring locations in the same object undergo the same or similar motions, while those in different objects have distinct motions. We therefore iteratively cluster the displacement vectors according to the principle of Minimum Description Length (MDL) (Rissanen 1978) to achieve segmentation. Two constraints are applied during grouping to ensure valid segmentation: the connectivity constraint requires that each recovered object be a connected component, and the motion constraint requires that multiple fragments with individual motions don't collide or inter-penetrate. The connectivity is maintained by merging neighboring objects in clustering. The enforcement of the motion constraint is based on Gottschalk's efficient use of the *separating axis theorem* for collision detection between two rectangular bounding boxes (Gottschalk et al. 1996).

Multi-resolution Scheme: We first sparsely estimate a displacement vector field at a large grid size and recover the fragmented concrete segments at a low resolution. This coarse result is used to estimate the displacement vector field at the smaller grid sizes, and to refine the boundary surfaces of fragments. This process continues until reaching the highest resolution.

Incremental Scheme: We recover the crack surfaces in an image sequence by processing every consecutive pair of images incrementally. We obtain a new displacement vector field by tracking the displacements of the same set of elementary regions. This scheme takes advantage of the longer image sequence for better motion estimation without additional processing.

Surface Extraction: The Marching Cubes algorithm (Lorensen and Cline 1987) is used to extract the triangulated crack surfaces by traversing every voxel. If a voxel contains a crack

2

surface, an 8-bit index is used to generate every triangle within the voxel by table lookup. The vertices of the triangles are derived by linear interpolation on the edges of the voxels.

EVALUATION

We transform a cylindrical concrete specimen of fixed size by two paradigms with pre-defined parameters (ground truth). In the first paradigm, the entire specimen is globally rotated and translated without generating cracks. In the second paradigm, the cylinder is separated into an upper and a lower portion by an artificially generated paraboloid crack. We recover these parameters using our method, and compare them with the ground truth.

Global Transformation Without Fragmentation

We globally transform the entire cylindrical specimen with a rotation followed by a translation. There are six parameters controlling the transformation. We specify the rotation using three Euler angles $\Theta = (\theta_x, \theta_y, \theta_z)$, first around x-direction, then y-direction, and finally z-direction, and the translation $T = (t_x, t_y, t_z)$. Ground-truth values of $\Theta = (1°, 2°, 3°)$ and $T = (4, 5, 6)$ (the units of translation are voxels) were chosen for testing.

The multi-resolution scheme is applied. From low to high resolutions, four displacement vector fields with an increasing number of displacements are obtained at the grid sizes of 64^3, 32^3, 16^3, and 8^3 voxels. The recovered parameters in each case are listed in Table 1. The recovered parameters approach the ground truth as the resolution increases.

TABLE 1. Comparison between the ground truth and the recovered parameters for a global transformation of a cylindrical specimen of concrete.

Grid size	64^3	32^3	16^3	8^3
$\theta_x = 1°$	1.002	0.997	0.999	1.000
$\theta_y = 2°$	1.991	1.995	1.998	2.000
$\theta_z = 3°$	3.012	2.995	2.994	2.995
$t_x = 4$	3.867	3.947	3.964	3.966
$t_y = 5$	4.986	4.997	5.003	5.009
$t_z = 6$	6.034	6.012	6.006	6.005

Simulated Fragmentation

In the simulated fragmentation, we generate a paraboloid crack inside the cylinder. This paraboloid separates the cylinder into a lower portion and an upper portion. The lower portion is rotated 3 degrees around the z-axis and shifted 5 voxels downward. The upper portion is rotated -3 degrees around the z-axis and shifted 5 voxels upward (Figure 2).
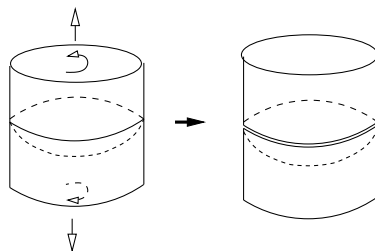
FIG. 2. Creation of cracks by a paraboloid-cut through a concrete cylinder. The upper and lower portions are rotated, and then shifted apart.

In addition to the motion parameters, we also test the accuracy of measuring the surface area of cracks approximated by triangulated surfaces. This surface area, computed analytically, is 6.92×10^5. The recovered parameters at increasing resolutions are listed in Table 2. All recovered motion parameters are close to the ground truth of Θ and T. The surface area of cracks has 5% error at the current highest resolution. This is the result of approximating smooth surfaces by flat triangulated patches. Figure 3 shows the visualization of triangulated surfaces of the upper and lower portions at the grid size of 8^3. The first picture shows both objects, the second and third picture shows each object individually.

TABLE 2. Comparison between the ground truth and the recovered parameters for fragmentation by a paraboloid crack in a cylindrical specimen.

Grid size	(Ground-truth)	64^3	32^3	16^3	8^3
	$\theta_x = 0°$	0.000	0.001	-0.001	-0.001
	$\theta_y = 0°$	-0.000	0.001	0.002	0.004
Upper	$\theta_z = -3°$	-3.008	-2.999	-2.998	-3.000
portion	$t_x = 0$	0.013	0.032	0.023	0.005
	$t_y = 0$	-0.001	-0.032	-0.044	-0.044
	$t_z = 5$	5.000	5.001	5.001	5.001
	$\theta_x = 0°$	0.003	-0.000	-0.001	-0.002
	$\theta_y = 0°$	-0.000	-0.002	-0.000	-0.001
Lower	$\theta_z = 3°$	3.008	3.000	2.999	3.000
portion	$t_x = 0$	-0.028	-0.041	-0.038	-0.023
	$t_y = 0$	0.046	0.039	0.039	0.028
	$t_z = -5$	-5.001	-5.000	-5.000	-4.999
Area of crack surface ($\times 10^5$)	6.92	4.28	5.66	6.80	7.28

FIG. 3. Visualization of triangulated surfaces at the grid size of 8^3. The first picture shows both objects, the second only the lower portion, and the third picture only the upper portion. The third picture is rotated differently.

MEASUREMENTS

We define the measures of crack surfaces based on the assumption that each crack consists of a pair of identical surfaces formed by the separation of fragments by rigid motions.

Number of Cracks: The number of cracks is obtained by first uniquely numbering each fractured segment, and then counting the different pairs of neighboring segments. The number of cracks is a global measure of the degree to which the specimen is fragmented.

Surface Area of Crack: The surface area of each crack is the sum of the area of all triangles in the two surfaces. As the paired surfaces are identical except for their locations, the surface area of the crack is twice the area of one surface, computed by summing the area of all of its constituent triangles. The area A of a triangle embedded in $\mathcal{R}^3$, specified by its three vertices $\mathbf{x}_1, \mathbf{x}_2, \mathbf{x}_3$, can be expressed as the magnitude of the cross product of its two edge vectors

$$A = |(\mathbf{x}_2 - \mathbf{x}_1) \times (\mathbf{x}_3 - \mathbf{x}_1)|/2. \tag{1}$$

Measuring the surface area of cracks is important because its growth indicates the generation of new cracks related to fracture energy. However, a crack can be widened without any change in its surface area. The following two measures address this issue.

Width of Crack: In our images, there is usually no significant relative rotation or shearing between pairs of crack surfaces. Therefore, we approximate the width of a crack at a specific location by the distance between the centroids of the corresponding triangles (Figure 4 (a)). If a pair of crack surfaces is parallel, uniform widths will be observed and the histogram of crack width will have a single peak. Otherwise, the histogram will be flat. We compute the histogram of crack widths to characterize the extent to which the crack surfaces are parallel.

Volume of Crack: Increases in volume indicate the generation of new cracks or the expansion of existing cracks. The volume of cracks can be calculated by summing the volumes of all twisted triangular prisms, formed by connecting the vertices of the corresponding pairs of triangles (Figure 4 (b)). The volume of each twisted triangular prism is the sum of the volumes of its three constituent tetrahedra (Figure 4 (c)). The volume V of a tetrahedron, specified by its four vertices at (x_i, y_i, z_i) where $i = 1, \cdots, 4$, is given by

$$V = \frac{1}{3!} \begin{vmatrix} x_1 & y_1 & z_1 & 1 \\ x_2 & y_2 & z_2 & 1 \\ x_3 & y_3 & z_3 & 1 \\ x_4 & y_4 & z_4 & 1 \end{vmatrix} \tag{2}$$

(a)   (b)   (c)
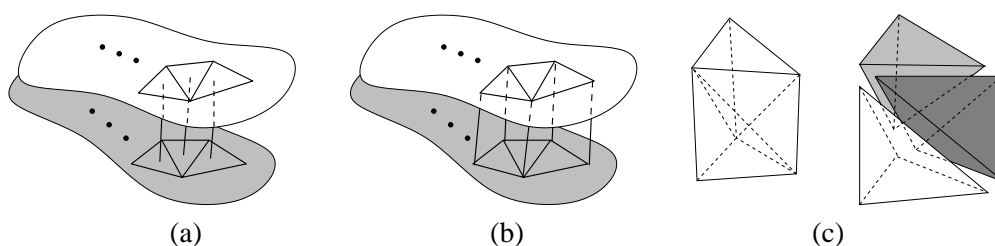
FIG. 4. Approximation of (a) the width of cracks by the distances between the centroids of corresponding triangles; (b) the volume of crack by summing the volumes of all twisted triangular prisms, formed by connecting the corresponding vertices between the pairs of triangles. (c) The volume of a triangular prism is calculated by summing the volumes of its three constituent tetrahedra.

Surface Tortuosity: Tortuosity is a measure of being twisted, crooked, and sinuous. We study the tortuosity of crack surface based on the surface normal ($\mathbf{n}$) and the two principal curvatures (k_1, k_2). At each point on a smooth surface, these properties are defined in differential geometry as follows: $\mathbf{n}$ is the normal direction of the tangent plane, and k_1, k_2 are the maximum and minimum curvatures of the set of curves crossing that point (Gray 1997). These geometric

quantities are reformulated as a spatial average at each vertex for a piece-wise linear triangular mesh. We define three measures of surface tortuosity:

1. $\mu_\theta^{\mathbf{n}}$: the average angle between every neighboring pair of surface normals. It will be zero on a flat surface, and within $(0, \pi]$ on a curved surface. $\mu_\theta^{\mathbf{n}}$ cannot characterize surfaces with distinctive properties of curvatures in different orientations. The curvature of a cylinder, for example, is positive along the circular, and zero along the lateral, direction.

2. μ_{k_1}, μ_{k_2}: the average principal curvatures. They are computed by summing the maximum and minimum principal curvatures at every vertex, and dividing the sums by the number of vertices.

3. $\sigma_{k_1}, \sigma_{k_2}$: the standard deviations of principal curvatures. They are useful as a measure of how "uniformly" k_1 and k_2 are distributed across the surface.

Permeability: Another important issue is the permeability of the specimen, whose change with crack growth affects the long-term durability of concrete. Permeability is here defined as the fraction of the volume at a given distance from the surface. We measure the permeability of a specimen by obtaining the distribution of this fraction over a range of distances. We obtain the distance of every voxel to the surface using the fast-marching level sets method. We initialize the level set at the boundary of specimen, and then shrink the level set at the constant speed of 1. After all interior voxels have been visited, we obtain each voxel's distance from the boundary.

RESULTS

Results from two sequences of concrete images, Sequence-B and Sequence-C, are presented. Sequence-B is composed of four images, referred to as B1, B2, B3, and B4. The size of each image is $704 \times 768 \times 512$. Sequence-C is composed of seven images, referred to as C1, C2, $\cdots$, C7. The size of each image is $704 \times 736 \times 608$. The volume of the shrink-wrapped concrete region is 1.2×10^8 in Sequence-B, and is 1.5×10^8 in Sequence-C [1].

TABLE 3. The number of cracks, crack area, crack volume, and the percentage of crack volume with respect to the total volume of concrete specimen.

| Image	B2	B3	B4	C2	C3	C4	C5	C6	C7
Number of cracks	1	5	18	0	3	6	23	18	29
Surface area of crack ($\times 10^5$)	6.1	8.9	15	0	12.6	18.4	37.1	39.6	43.5
Volume of crack ($\times 10^5$)	4.9	30	84	0	23.9	45.9	140.7	207	270
% of total concrete volume	0.4	2.5	7	0	1.5	3.0	9.1	13.3	17.5

Number of Cracks: Various properties of crack surfaces are listed in Table 3. In both sequences, we observe a sudden increase in the number of cracks. In Sequence-B, the specimen is separated into two parts in B2, thus only one crack is identified. Five cracks are identified in B3. The number jumps to eighteen in B4. In Sequence-C, no crack is found in C2 as it is globally transformed C1. Three and six cracks are obtained in C3 and C4. This number jumps to around 20 to 30 in C5 through C7.

Surface Area and Volume: The increases in the surface area and volume indicate the generation of new cracks and the expansion of existing cracks. The volume of cracks is relatively small

---

[1]The unit of volume is the volume of a voxel. The unit of area is the area of a voxel face. The unit of width is the length of a voxel edge.

compared to the entire volume of interest. Even in B4 of Sequence-B, the cracks only cover 7% of the concrete specimen. In Sequence-C, this percentage remains small. Among C5, C6 and C7, the rates of increase in the volume is much larger than those in the surface area: indicating expansion of existing cracks without creation of large new cracks.

Histograms of Crack Widths: In order to compare the widths of different cracks, a uniform bin size (half a voxel width) was selected to generate the histograms of crack widths. Due to the limited space, we only display the histograms of crack widths of the largest four cracks in B3 in Figure 5. Both parallel cracks (highly peaked) and non-parallel cracks (flat) can be observed. Cracks from other specimens have similar properties.
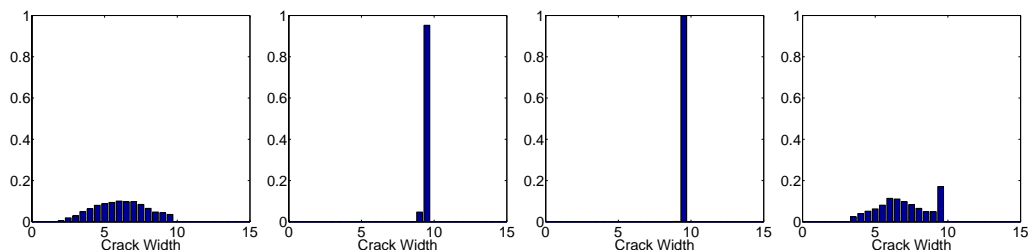
FIG. 5.   The histograms of crack widths among the largest four cracks in B3.

Surface Tortuosity: Measures of tortuosity on the crack surfaces are in Table 4. We list only the results of the largest crack in each specimen. Despite their different sizes and locations, all cracks have similar values in every measure. The values of $\mu_\theta^{\mathbf{n}}$ are relatively large, and μ_{k_1}, μ_{k_2} have opposite signs. This indicates that the crack surfaces have bumps and dents of small amplitudes. The values of the principal curvatures are less than those of the corresponding standard deviations, indicating the wide scattering of bumps and dents across the crack surface.

TABLE 4.   Measurements of tortuosity of the crack surfaces.

	B2	B3	B4	C3	C4	C5	C6	C7
$\mu_\theta^{\mathbf{n}}$	0.42	0.35	0.35	0.46	0.49	0.51	0.52	0.53
μ_{k_1}	0.030	0.023	0.022	0.069	0.070	0.071	0.065	0.080
σ_{k_1}	0.046	0.032	0.031	0.102	0.110	0.109	0.102	0.113
μ_{k_2}	-0.033	-0.023	-0.022	-0.062	-0.068	-0.066	-0.078	-0.068
σ_{k_2}	0.046	0.032	0.031	0.101	0.111	0.108	0.104	0.109

Permeability: Figure 6 shows the changes of permeability as a result of fragmentation at slice 256 in every image of Sequence-B, where darker pixels indicate larger, and brighter pixels smaller, distances from the boundary. As fragmentation progresses, the permeability increases because the surfaces get closer to more voxels.

CONCLUSION

We have developed a motion-based method to extract the crack surfaces from X-ray micro-tomographic concrete images. We demonstrated that various measures can be obtained from the approximation of cracks by triangulated meshes, including the number of cracks, surface area, volume, tortuosity, and permeability. Results show that there are relatively few large cracks, parallel or non-parallel. The crack surfaces, despite their different sizes and spatial locations, have very similar properties in surface tortuosity. They are locally tortuous with bumps

| B1 | B2 | B3 | B4 |
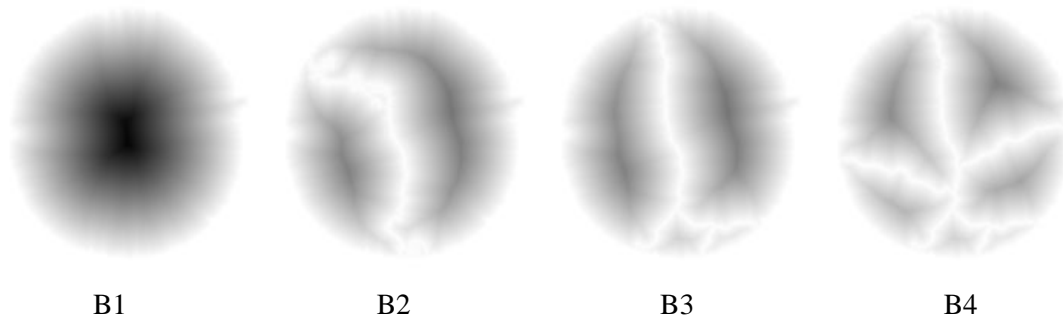
FIG. 6. Permeability of slice 256 in every image of Sequence-B. Darker pixels indicate larger, and brighter pixels smaller, distances from the surface.

and dents, but still quite "flat" globally. Finally we demonstrated the increase of permeability with fragmentation. These new 3D measurements may help material scientists to improve the characterization of concrete fracture.

REFERENCES

Barnea, D. I. and Silverman, H. F. (1972). "A class of algorithms for fast digital image registration." *IEEE Transactions on Computers*, C-21(2), 179–187.

Bažant, Z. P. (1995). "Scaling theories for quasibrittle fracture: recent advances and new directions." *Fracture mechanics of concrete, Proc., 2nd Int. Conf. on Fracture Mech. of Concrete and Concrete Structures (FraMCoS-2)*, F. Wittmann, ed., ETH, Zürich. Aedificatio Publishers, 515–534.

Gottschalk, S., Lin, M. C., and Manocha, D. (1996). "Obbtree: a hierarchical structure for rapid interference detection." *Proceedings of the 23rd Annual Conference on Computer Graphics and Interactive Techniques*. 171–180.

Gray, A. (1997). *Modern Differential Geometry of Curves and Surfaces with Mathematica*. CRC Press, 2nd edition.

Konrad, J. (2000). "Motion detection and estimation." *Handbook of Image and Video Processing*, A. Bovik, ed., Academic Press Series in Communications, Networking and Multimedia, Academic Press, chapter 3.10, 207–225.

Landis, E. N., Nagy, E. N., Keane, D. T., and Nagy, G. (1999). "Technique to measure 3d work-of-fracture of concrete in compression." *Journal of Engineering Mechanics*, 125(6), 599–605.

Lorensen, W. E. and Cline, H. E. (1987). "Marching cubes: a high resolution 3d surface construction algorithm." *ACM Computer Graphics (Proceedings of SIGGRAPH '87)*, 21(4), 163–169.

Malladi, R., Sethian, J. A., and Vemuri, B. C. (1995). "Shape modeling with front propagation: A level set approach." *IEEE Transactions on Pattern Analysis and Machine Intelligence*, 17, 158–175.

Rissanen, J. (1978). "Modeling by shortest data description." *Automatica*, (14), 465–471.

Zhang, T. (2004). "Identification of structural changes from volumetric image sequence," PhD thesis, Department of Electrical, Computer, and Systems Engineering, Rensselaer Polytechnic Institute.